JCI insight

# A Porcine Commotio Retinae Model for Pre-clinical evaluation of Post Traumatic Photoreceptor Degeneration

Juan Amaral, Irina Bunea, Arvydas Maminishkis, Maria M. Campos, Francesca Barone, Rohan Gupta, Mitra Farnoodian, Jonathan Newport, M. Joseph Phillips, Ruchi Sharma, David M. Gamm, Kapil Bharti, Richard J. Blanch

*JCI Insight*. 2026. https://doi.org/10.1172/jci.insight.192799.

**Research** In-Press Preview **Neuroscience** **Ophthalmology**

Commotio retinae (CR) resulting from retinal trauma can lead to focal photoreceptor degeneration and permanent vision loss. Currently no therapies exist for CR-induced retinal degeneration, in part due to a lacking large animal model that replicates human injury pathology and allows testing of therapeutics. Severe CR is clinically characterized by subretinal fluid and focal photoreceptor outer nuclear layer thinning. To develop a porcine CR model, we developed a laser-guided projectile apparatus and optimized projectile delivery procedure using porcine cadaveric eyes embedded in a 3D-printed porcine skull. Scleral and corneal impacts, resulted in retinal damage consistent with patient injury but corneal impacts also led to cornea damage and opacification, which precluded follow up imaging. In live porcine eyes, scleral impacts of 39.5 m/s induced transient blood retinal barrier breakdown evidenced by subretinal fluid on optical coherence tomography (OCT), leakage observed on fluorescein and indocyanine green angiography, and transient photoreceptor outer segment disruption seen by OCT and multifocal electroretinography. Impacts above 39.5 m/s induced longer-lasting photoreceptor degeneration, but only transient blood retinal barrier breakdown. This porcine model, combined with clinically relevant imaging and diagnostic modalities will be valuable for testing the safety and efficacy of therapies to restore vision after focal photoreceptor degeneration.

# A Porcine Commotio Retinae Model for Pre-clinical evaluation of Post Traumatic Photoreceptor Degeneration

Juan Amaral[1], Irina Bunea[2], Arvydas Maminishkis[1], Maria M. Campos[3], Francesca Barone[2], Rohan Gupta[2], Mitra Farnoodian[2], Jonathan Newport[4], M. Joseph Phillips[5,6], Ruchi Sharma[2], David M. Gamm[5-7], Kapil Bharti*[2], Richard J. Blanch*[8-10]

1: NEI/ Translational Research Core/OGVFB, Bethesda, MD, USA

2: NEI/OSCTRS/OGVFB, Bethesda, MD, USA

3: NEI/Biological Imaging Core/Histology core, Bethesda, MD, USA

4: NEI/ Laboratory of Sensorimotor Research, Bethesda, MD, USA

5: Waisman Center, University of Wisconsin- Madison, Madison, WI, USA

6: McPherson Eye Research Institute, University of Wisconsin-Madison, Madison, WI, USA

7: Department of Ophthalmology, University of Wisconsin-Madison, Madison, WI, USA

8: Academic Department of Military Surgery and Trauma/Royal Centre for Defense Medicine, Birmingham, United Kingdom

9: Neuroscience and Ophthalmology, School of Infection, Inflammation, and Immunology, University of Birmingham, Birmingham, United Kingdom

10: Department of Ophthalmology, University Hospitals Birmingham NHS Foundation Trust, Birmingham, United Kingdom

*Corresponding authors:

**Kapil Bharti**

10 Center drive, Bldg 10, Rm 10B10, Bethesda, MD 20892; kapil.bharti@nih.gov; +1-3014519372

**Richard Blanch**

FRCOphth, Neuroscience and Ophthalmology, Institute of Inflammation and Ageing, University of Birmingham, Birmingham B15 2TH, United Kingdom. blanchrj@bham.ac.uk; +44 (0)121 414 3344

**Keywords**

Pig model, age-related macular degeneration, large animal model, cell therapies, gene therapies, tunable outer retinal degeneration, battle-field injuries, military trauma

**Abstract**

Commotio retinae (CR) resulting from retinal trauma can lead to focal photoreceptor degeneration and permanent vision loss. Currently no therapies exist for CR-induced retinal degeneration, in part due to a lacking large animal model that replicates human injury pathology and allows testing of therapeutics. Severe CR is clinically characterized by subretinal fluid and focal photoreceptor outer nuclear layer thinning. To develop a porcine CR model, we developed a laser-guided projectile apparatus and optimized projectile delivery procedure using porcine cadaveric eyes embedded in a 3D-printed porcine skull. Scleral and corneal impacts, resulted in retinal damage consistent with patient injury but corneal impacts also led to cornea damage and opacification, which precluded follow up imaging. In live porcine eyes, scleral impacts of 39.5 m/s induced transient blood retinal barrier breakdown evidenced by subretinal fluid on optical coherence tomography (OCT), leakage observed on fluorescein and indocyanine green angiography, and transient photoreceptor outer segment disruption seen by OCT and multifocal electroretinography. Impacts above 39.5 m/s induced longer-lasting photoreceptor degeneration, but only transient blood retinal barrier breakdown. This porcine model, combined with clinically relevant imaging and diagnostic modalities will be valuable for testing the safety and efficacy of therapies to restore vision after focal photoreceptor degeneration.

## Introduction

Traumatic retinopathy is a significant cause of vision loss and blindness, with eye injury–associated vision impairment affecting 4.5 per 1,000 Americans. Among those affected, 5.1 per 1,000 experience unilateral blindness, and 4.5 per 10,000 have bilateral blindness (1-3). Globally, 55 million eye injuries occur annually, resulting in bilateral visual impairment in 2.3 million people and unilateral blindness or low vision in nearly 19 million individuals (4, 5). Furthermore, traumatic vision loss is often acute (4), affects relatively younger individuals, is associated with occupational and psychiatric complications, and contributes significantly to lost productivity and reduced quality of life (6).

One form of traumatic retinopathy is commotio retinae (CR), a condition affecting the outer retina, associated with temporary or permanent visual function loss following a closed-globe injury (7-11). The incidence of CR in civilian population is approximately 0.4%, but it accounts for up to 15% of military ocular trauma cases and leaves a significant number of veterans with lifelong visual impairment (8, 10, 12). In real-world scenarios, the location of impact leading to CR is sporadic, unpredictable and often unknown. Depending upon the location, the damage can also be variable. Of concern are the CR cases where the macula is involved – in such cases visual acuity can be significantly reduced without any treatment possibility. Macular CR can occur after anterior segment trauma (*contra-coup*) or direct scleral impact (13, 14). After macular CR, 15-20% of patients suffer permanent visual impairment, primarily related to photoreceptor degeneration (7, 8, 15). Rats, rabbits, cats, pigs, and rhesus and owl monkeys have been used as animal models for commotio retinae (15-27), however, none fully or consistently replicate the macular pathology observed in human injury. Some models, such as rabbits and rat, lack a macula-homologue, while others, such as pigs and non-human primates that have a macula homolog, were developed predominantly with direct peripheral injuries rather than central (where

energy of impact transmitted to macular region) as seen in the human CR pathology. Another unresolved aspect of CR injury is the nature of Berlin's edema, which has been described as a hallmark feature of CR pathology (28). But there is ongoing debate about the degree to which the outer blood-retinal barrier is disrupted following CR injury (16, 18, 20, 23, 29, 30). The heretofore inability to perform clinically relevant longitudinal live imaging modalities has further limited translation of previous CR models to test human relevant treatment modalities. Moreover, because CR injury can affect a relatively large retinal area—including the entire macula (up to 20 $mm^2$) - there is a clear need for a large animal model of CR that accurately replicates human closed-globe macular injury. Such a model would enable proper characterization of the injury response and facilitate testing of clinically relevant imaging techniques and allow preclinical evaluation of regenerative therapies aimed at replacing lost photoreceptors and/or restoring photoreceptor function through other approaches.

Pigs are an ideal preclinical animal to develop such a model, as the porcine eye lacks a tapetum, has a human comparable average axial length of 23.9 mm, and a holangiotic retinal blood supply with a capillary meshwork of similar caliber that supplies identical retinal layers as in human eyes (31). While pigs don't have a macula, they have a central visual streak rich in cone photoreceptors (31, 32). Because of their comparability to human eyes, pig eyes are suitable for surgical procedures such as vitrectomy and subretinal transplantation of large constructs that can cover a significant portion of the macula (33, 34). Furthermore, pigs are significantly more cost effective and easier to handle and obtain as compared to non-human primates (33, 35, 36).

Using a scleral impact approach, we developed a closed-globe macula-injury specific CR pig model to characterize the acute and chronic injury response. Scleral impact allowed us to test clinically relevant imaging modalities, not feasible with corneal impact (36, 37), such as optical coherence tomography (OCT), OCT angiography (OCTA), fluorescein and indocyanine green angiography (FA/ICG-A), and multifocal electroretinography (mfERG) to evaluate and diagnose

the cone photoreceptor response to injury. Our data suggest that the porcine CR model closely mimics the human macular CR injury, mimicking the human closed-globe macular CR injury. Our model showed retinal whitening, preretinal hemorrhage, transient outer blood retinal barrier breakdown, and progressive photoreceptor outer segment degeneration – symptoms seen in patients with a CR injury. This clear longitudinal analysis is useful for the development of treatments for severe macular CR and may aid in the development of treatments for other forms of outer retinal degenerations.

## Results

### Development of a pressure application device (PAD) for inducing closed-globe CR injury

To develop a reproducible closed-globe CR porcine model that mimics human macular CR injury, we developed a pressure application device (PAD) that is used to injure the eye using a fixed diameter projectile impact. To induce injury, PAD delivers predetermined energy by propelling a plastic projectile (ø12mm) towards the pig eye at a measured speed using a laser-guided mechanism. The PAD was designed as a closed pneumatic system that operates using compressed nitrogen gas to generate precise pressure (measured in PSI) that can be reproducibly applied to a propel a plastic ball at a specific speed (measure in m/s). To accurately target the injury location at the visual streak, the eye fundus was visualized using binocular indirect ophthalmoscopy and different projectile impact areas (cornea, limbus, and sclera) were tested. The plastic ball is “loaded” into acceleration tube using the loading port; then, propelled using pressure from the compressed nitrogen gas and a solenoid-actuated fast opening valve with remote trigger; tube is aimed at the desired location using the laser beam (Fig. 1A, Supplementary Video 1, Supplementary Figs. 1A, B). The impact of the plastic ball transfers its kinetic energy to the eye, modelling blunt force or concussive injury such as after a blast (Fig. 1B). To determine projectile speed reproducibility, we evaluated linearity between PSI and projectile speed (Supplementary Fig. 1B) and confirmed a linear relationship between PSI and the projectile speed within the range of pressures tested for the projectile release (Fig. 1C). This data confirms our ability to deliver the projectile consistently at a specific speed.

### *Ex vivo* Evaluation of PAD Induced CR

To develop an animal model with reproducible macular CR injury, we set out to optimize the injury location that would lead to ellipsoid zone (inner outer segments of the photoreceptors) and photoreceptor outer nuclear layer (ONL) damage in pig's visual streak. With the goal of reducing the number of animals, we chose to perform initial testing of optimal injury location and projectile speed *ex vivo* on cadaveric pig eyes. Since slaughterhouse eyes lack the orbital support (muscle, fat, ligaments, optic nerve), to reduce artificiality of an *ex vivo* model and to mimic as closely possible the *in vivo* environment, we developed a 3D-printed pig skull in which we mounted the cadaveric pig eyes. A high-resolution computer tomography (CT) scan of a pig head was performed and was used to construct a 3D image of the pig skull using the CT scan software (Fig. 2A). This 3D image was used to 3D-print a pig-skull. The skull was printed commercially using material that has similar mechanical properties to bone (https://www.anatomicalworldwide.com) (Fig. 2B). A ballistic gel® (see methods) made from synthetic gelatin was used to fill the 3D printed pig skull, mimicking the elastic properties of the orbital and cranial tissues, thus explicitly helping assess the impact of projectile kinetic energy transfer to the eye simulating what happens in a live animal and human injury. Freshly obtained cadaveric pig eyes were placed in the eye sockets of the 3D-printed pig skull (Figs. 2C; Supplementary Figs. 2A, B). Despite lacking anatomical structures around the eye (muscles, blood vessels, and the fat deposits), these cadaveric eyes provided the first best approximation of injury location and impact intensity allowing us to rule out conditions incompatible with our goal of central retinal injury with minimal corneal damage. PAD was used to deliver projectiles at different speeds to determine the optimal speed and the optimal impact location (Fig. 2C). Injury damage was evaluated by gross evaluation in dissected eyes and by histology (Figs. 2D-H, Supplementary Figs. 2, 3). We first tested the hypothesis that direct corneal impacts can lead to visual streak damage. With projectile speed of 40.5 m/s, although we detected damage to the retina and the visual streak, the impact caused retinal folds and

discernable damage to the cornea with epithelial displacement (Figs. 2D, E; Supplementary Figs. 2C, D; Supplementary Table 1). Since retinal folds were not a desired outcome and corneal damage would preclude longitudinal live imaging, we didn't pursue this approach further. Next, we asked whether projectile impacts at the limbus will damage the retina. Unexpectedly, limbal impacts with projectile speed of 40.5 m/s only a peripheral damage to the cornea was induced and a peripheral retinal dialysis (retinal tear at the *ora serrata*) was also seen (Supplementary Figs. 2E, F; Supplementary Table 1). This led us to test whether direct scleral impacts could result in desired retinal damage. With progressively increasing projectile speed from 33-40 m/s damage to the retina at the impact site increased from displacement of retinal layers at 33 m/s; edema and fibrosis at 35.7 m/s to almost complete retinal atrophy at 40 m/s (Supplementary Figs. A-E). In comparison, in the visual streak, projectile speeds at and below 39.5 m/s caused desired damage to the ellipsoid zone and the ONL, whereas speed of 40 m/s or more caused atrophic changes and retinal folds, as well random preservation of retinal structures outside the impact area (Figs. 2F-H; Supplementary Figs. 3F-J; and Supplementary Table 1). Based on our analysis of cadaveric pig eyes, we hypothesized that, living pig eyes will be more sensitive to scleral damage, so relatively lower velocities will be required to damage the visual streak area and minimize collateral damage to the anterior segment of the eye that will preclude longitudinal post-injury evaluations.

**Acute Outer Blood Retinal Barrier (oBRB) Damage in PAD-induced CR**

Based on our *ex vivo* analysis, we began testing on living pig eyes with projectile impact speed of 35.7 m/s. Five pigs were enrolled in this study. In all cases, fundus examination immediately after injury revealed the presence of preretinal hemorrhage at the area of impact (zone 1) and retinal whitening adjacent to it (zone 2) (Fig. 3A). There was extensive oBRB breakdown at zone 1 extending into zone 2, as evidenced by fluorescein leakage within a min after dye injection

continuing until the 10-minute evaluation time point (Figs. 3B, C; left panels). ICGA changes were minimal, suggesting no disruptions in retinal or deeper choroidal vessels (Figs. 3B, C; right panels). Fluorescein Leakage subsided within 8-11 days post-injury, suggesting a transient disruption of the oBRB with no additional changes in ICGA (Figs. 3D-E). OCT examination immediately after the injury revealed retinal detachment and subretinal fluid accumulation at the site of impact extending into zone 2 (Figs. 3F, G). OCT analysis also revealed extensive ellipsoid zone disruption extending from zone 2 into the visual streak (zone 3) (Figs. 3F, G). Quantification of OCT data revealed a range of sizes for different zones illustrated in Fig. 3F (zone 1: 2.0-4.0 mm; zone 2: 3.0-8.0 mm; zone 3: 2.0-8.0 mm). These findings were confirmed by histological analysis of the cadaveric pig eyes four days after the CR injury, revealing preretinal hemorrhage and extensive retinal damage with retinal atrophy in zone 1, thinning of outer retina and layer disorganization in zone 2, and photoreceptor disruption extending away from this area (Fig. 3H). Follow-up by OCT confirmed FA/ICGA findings revealing subretinal fluid accumulation seen at day 0 (Figs. 3I, J) that was resolved in the first 2 weeks (Fig. 3K). Interestingly, disruptions of the ellipsoid zone seen on day 0 persisted beyond day 14 (Figs. 3J-L). These findings were further confirmed by histological analysis of the retina (Figs. 3M, N), where photoreceptor outer segments shortening and ONL thinning and disruptions was evident. mfERG analysis showed reduced signal in the visual streak, confirming functional defects in cone photoreceptors (Supplementary Fig. 4; Figs. 3O,P). Overall, our data suggest that with impact speed up to 35.7 m/s, there was an acute oBRB breakdown that recovered by day 11, while the ellipsoid zone disruptions persisted.

**Long-term Photoreceptor Damage in PAD-induced CR**

Short-term evaluation of the CR injury provided findings that were consistent with the patient data in terms of specificity of damage to photoreceptors(7, 38-43). Short-term evaluation also revealed acute oBRB damage not previously described for CR patients. With the goal of developing a

suitable large animal model for testing potential therapies, next we set out to determine if PAD-induced CR injury at a projectile speed of 35.7 m/s persists longer term. Five pigs were enrolled in this part of the study and evaluated for up to 60 days after injury. As seen in the short-term studies, in all cases there was preretinal hemorrhage (zone 1) and retinal whitening - likely associated with an acute oBRB breakdown, which progressively healed by 16 days, as confirmed by fluorescein angiographs (Figs. 4A, B, D, E). ICGA changes continue to be unremarkable by day 16 of evaluation, suggesting no damage to retinal or choroidal vessels (Figs. 4B, E). OCT analysis confirmed sub retinal edema on day 0 in zone 2, which reabsorbed by day 16 (Figs. 4C, F). Surprisingly, the ellipsoid zone disruption evident in higher magnifications at day 15, recovered by day 30 (compare Figs. 4G with H and I). This transient structural defect and its recovery was corroborated by initial loss and subsequent recovery of the mfERG signal, measured over the visual streak area (Figs. 4J-L). Because of this finding, we decided to increase the projectile impact speed to 39.5 m/s. Expectedly, higher speed caused deeper impact that was evident even at the 60 days follow up and there was no recovery of the ellipsoid zone on OCT (Figs. 4M, P). However, this high impact led to higher variability in structural damage to the retina with larger areas of retinal atrophy and relatively smaller EZ disruption areas as assessed by OCT (compare Figs. 4M, P); variable non-perfusion of the choriocapillaris as seen by OCTA (compare Figs. 4N, Q), and variable functional changes in the visual streak as seen by mfERG (compare Figs. 4O, R). This variability, combined with the evidence of collateral damage to the posterior lens capsule and anterior segment (Supplementary Fig. 5), prompted us to seek an alternative impact method to generate more reproducible, long-term, and specific injury to the photoreceptors without extensive anterior segment collateral damage.

## Scleral Patch Improves Reproducibility of the CR injury

During post hoc analysis of evaluated eyes and based on literature evidence of variable scleral thickness in pigs, we asked if we could control variability in injury extent by temporarily adding a scleral patch to the injury location (44). We used a commercially available cadaveric human scleral patch and glued it to the posterior sclera by disinsertion of the median rectus and release of the limbal traction (see Methods for surgery details). After the impact, cadaveric scleral patch was removed, and median rectus was re-sutured back to sclera (Figs. 5A-D, Supplementary Fig. 6).

Four pigs were subjected to a projectile impact at a speed of 39.5 m/s and monitored for up to 60 days post-injury. As seen with injury without the scleral patch, preretinal hemorrhage (zone 1) and retinal whitening (zone 2) seen immediately after the impact was also seen with the scleral patch, by color fundus photography (Fig. 6A). Fluorescein angiography confirmed retinal whitening was caused by oBRB disruption (Fig. 6B – left panel). Similar to the CR injury without the scleral patch, ICGA didn't show any signal suggesting no damage to the choroidal vessels (Fig. 6B, right panel). Edema seen on day 0 by OCT analysis resolved by day 30, suggesting oBRB heals by this time. (Figs. 6D and E). In contrast, the ellipsoid zone disruption continued beyond day 30 until day 60 evaluation timepoint (Figs. 6D-F). OCT angiography revealed a non-statistically significant decrease in CC density in the first 15 days after injury, with partial recovery by 60 days (Figs. 6G-J).

To confirm reproducibility of this approach, we compared OCT data across four eyes. As expected, by day 60 edema seen after projectile impact was reabsorbed (Supplementary Fig. 7). The area of the impact showed noticeable retinal degeneration, and the adjacent area showed progressively improving retinal thickness with consistently missing ellipsoid zone (Supplementary Fig. 7). To quantify changes seen in OCT, we performed segmentation of retinal layers using our recently published AI-based algorithm for OCT segmentation (34). Segmentation analysis

confirmed that use of the scleral patch results in a milder (~20%) reduction in ONL thicknesses as compared to injury without the patch (~50% reduction in ONL thickness) (Fig. 6K). Multifocal ERG heatmap analysis showed a corresponding decrease in signal, persisting up to 60 days (Fig. 6L-N), consistent with longer term photoreceptor damage. Our results indicate that the addition of a scleral patch to the impact area generated reproducible visual streak lesions and yielded a model that allows better understanding of human CR injuries and will help develop effective therapies for photoreceptor degeneration.

**Histologic evaluation of PAD-induced CR injury to the retina**

To further evaluate the impact of CR injury on porcine retina, we performed histological analysis of eyes at the end of 60 days of longitudinal live imaging. Consistent with the OCT data (Fig. 7A), histological (Figs. 7B-F) and immunostaining analysis provide qualitative analysis of three distinct areas of injury (Figs. 7G-J)**.** The impact zone: H&E staining showed complete atrophy of both inner and outer retinal layers (compare Figs. 7B, C and F); immunostaining further confirmed missing signals for cone photoreceptors (PNA) and RPE (RPE65) (compare Figs. 7G-J). A transition zone: H&E and immunostaining showed partial preservation of the inner retina and rosette-like structures with disruptions in outer retinal layers including the RPE, OS, and ONL; barely visible RPE layer with faint RPE65 immunostaining and no PNA signal suggesting missing cone photoreceptor outer segments (compare Figs. 7B, D and F and 7H and J). The EZ disruption zone with a thinned ONL, lacking PNA signal but relatively intact RPE and INL (compare Figs. 7B, E and F and 7I, J). Overall, this histological analysis (H&E and immunostaining) corroborated our *in vivo* structural and functional evaluations, confirming the loss of photoreceptors for the evaluation period of up to 60 days in PAD-induced closed-globe CR injury.

## Discussion

We report a reproducible large animal model of post traumatic photoreceptor degeneration that mimics macular injury seen in patients with closed-globe CR injuries. Injury in this porcine model recapitulates several features of the human macular CR injury, including: **1)** involvement of the macula-equivalent visual streak in pigs; **2)** a transient oBRB breakdown; **3)** a transient subretinal fluid accumulation that resolves by 7-14 days; **4)** with lower energy projectile impacts (at or below 38 m/s projectile speed), damage is limited to photoreceptor outer segments and recovered by 30 days post injury; **5)** damage caused by projectile impact speed of 39.5 m/s leads to persistent absence of the ellipsoid zone and ONL thinning for the entire evaluation period of 60 days, suggesting permanent damage.

Commotio retinae was originally named Berlin's oedema and was described as retinal whitening involving loss or disruption of photoreceptor outer segments (28, 45). Previous reports of oBRB breakdown in closed-globe injuries have been contradictory. In a series of 21 patients evaluated with FA and ICGA, findings varied (46). More specifically, fluorescein dye leakage occurred in nine out of 21 eyes, and a "salt and pepper" appearance was observed in one, which the authors felt indicated a more severe injury (though visual acuity was not reported in these cases). In some cases, the early increase in choriocapillaris permeability developed into choriocapillaris vascular occlusion by day four. In cases where evaluated, abnormal FA and ICGA showed delayed filling of CC (20, 22-24, 29, 45, 46). This finding led the authors to speculate that in severe CR, occlusion of the choriocapillaris causes outer retinal ischemia, impairing recovery. More recent studies report subretinal fluid (SRF) only in the most severe injuries (29). In comparison to these previous reports, in our model, oBRB breakdown and SRF was seen in all cases, including those that do not recover defects in outer retina structure and function. It is likely that previous reports, in which patients were assessed at variable times after injury, transient and localized (outside the

posterior pole) oBRB breakdown may have been missed. Another possible reason for this discrepancy may have to do with location of injury, which is variable in human blunt force injuries. Our ability to generate a reproducible injury, combined with our subsequent systematic and comprehensive analysis, leads us to speculate that oBRB breakdown may be a common, if not a universal, feature of CR injuries, and that the loss of the choriocapillaris does not directly correlate with outer retina damage or its recovery. While retinal detachment in the context of severe ocular trauma is a concern, acute SRF accumulation after blunt trauma at the site of commotio or sclopetaria retinae may be serous, as indicated by previous studies (46, 47). But the oBRB breakdown seems to resolve with time for most cases. This finding is consistent with published clinical reports (20), supporting the transient nature of the oBRB breakdown.

The impact sites and speed reported in previous animal models of commotio retinae (47) are variable, but in general, higher speed impacts of low weight projectiles were shown to cause persistent and reproducible CR injury as compared to lower speed impacts from heavy projectiles that caused more damage at the impact site and the neighboring retina (16, 19, 21, 27). Higher projectile speed produces desired damage in our model; however, the site of injury was critical in obtaining a reproducible and retina specific damage. We used a scleral injury site because corneal impacts with energies sufficient to induce commotio retinae also damaged the anterior segment - inducing corneal edema, cataract, iridodialysis and hyphema. These anterior segment disruptions preclude proper evaluation of the retinal damage using clinically relevant imaging modalities such as OCT, OCT-A, mfERG, FA/ICGA. Scleral impacts not only avoid anterior segment disruption but also produce the same ultrastructural features of CR injury seen in patients. Putting together these findings, scleral impact induced closed-globe CR injury provides a more clinically relevant and reproducible animal model for better understanding CR etiology and for testing injury-specific therapeutic approaches.

At optimized projectile speeds, photoreceptor outer segment damage was visible after one week of injury and continued for the two-month evaluation period. Our OCT findings are consistent with previous reports (38-42, 48); namely, with projectile speed of 37.5 m/s or less, there was an initial increase in reflectivity of the inner/outer segment ellipsoid zone with disappearance of the thin hyporeflective optical space. In these cases, OCT changes recovered over time. With projectile speed of 39.5 m/s, OCT revealed disruption of the inner and outer segment layers with partial atrophy of the outer nuclear layer, and no recovery of the ellipsoid zone and the ONL during the evaluation period of 60 days. These results are consistent with Chen et al., who found that foveal thickness and grade of outer retinal atrophy were predictors of final visual outcome(8, 41). The ellipsoid zone and ONL thinning in the macular area may therefore also help predict which patients could benefit from what kind of therapies.

Our mfERG findings are also in agreement with previous reports of transient decrease in mfERG amplitude with lower projectile speed (43, 49). With projectile speed of 37.5 m/s, the mfERG amplitude reduced significantly after the injury but recovered over a 30-day period while with projectile speed of 39.5 m/s, the mfERG amplitude remained low for the entire evaluation period of 60 days. Similar to Mansour et al (50), we report the presence of pre-retinal, retinal, and subretinal hemorrhage around the area of impact as seen by fundus imaging and histology. The preretinal hemorrhage being sub-hyaloid could explain its rapid reabsorption in our cases (11). Furthermore, we provide the first immunofluorescence findings in a CR injury, confirming that photoreceptor degeneration occurs while RPE cells remain viable 60 days after injury. Overall, our model confirms what has been reported in previous rodent models of CR injury but also furthers the field with findings that are consistent with the human injury.

Our model has several advantages over previous CR models: **1)** the pig eye is similar in size and retinal structure to the human eye (32); **2)** the pig visual streak is cone rich, like the human macula; **3)** using a posterior scleral injury approach, we were able to preserve the health and transparency of the cornea and the lens, allowing us to perform longitudinal structural and functional assessment of the retina using clinically relevant imaging modalities; **4)** retinal analysis led us to discover three discrete areas, the impact zone, the transition zone - an area adjacent to the direct impact site where the damage to the ONL and ellipsoid zone was extensive, and the EZ disruption zone with photoreceptor specific damage to the ellipsoid zone and the ONL. One limitation of our model is that it may not fully capture the disease-associated pathophysiology of photoreceptor-specific retinal degeneration. Therefore, it will be important to also evaluate photoreceptor transplants in disease models, such as the P23H rhodopsin mutation model of retinitis pigmentosa (51). Nonetheless, our model represents a valuable platform for advancing the development of vitreoretinal surgical techniques, instrumentation, and potential therapies for photoreceptor degeneration.

## Methods

### Study design

All animals received a baseline examination prior to the CRR injury, including OCT, OCTA FA/ICG-A and mfERG. The same examinations were repeated immediately after the CR injury and at around 7-11, 15, 30 and 60 days after. Because of logistics of animal handling, different animals could not be followed on the same day. Hence, they were followed within a window of a few days. Animals were euthanized at different time points up to 60 days, and the eyes were collected for histology (H&E, Masson and immunofluorescence evaluation).

**Sex as a biological variable** Sex was not considered as a biological variable. CR injury is not anticipated to be different between males (castrated or non-castrated) and females. Castrated males were used for this study because only they (not non-castrated males or females) are amenable to social housing, allowing an enriched social environment for the animals (52).

### Animal care and procedures

Yorkshire and Yucatan minipigs from Premier BioSource/S&S Farms and Sinclair Research were enrolled in the study. Since pig eyes are fully developed by 6 months, the only limitation for long-term evaluations between both breads was the rate of growth which was slower in the Yucatan breed. Animals (castrated males, 35-45 Kg) were housed in climate control rooms illuminated at 25-37 lux with a 12 hours on-cycle and wood shavings on the floor. Food was provided twice a day, and water was offered *ab libitum*. For imaging and CR injury, pigs were anesthetized, intubated, and maintained on a pressure-controlled ventilator, as previously described (52). Pigs were positioned in custom cradles and water, and air-warming blankets were used to maintain the body temperature. Blood pressure, heart rate, blood oxygenation, $CO_2$, and temperature were monitored continuously. Sodium chloride (0.9% sodium chloride injection USP, Hospira) or lactated Ringer's (Lactated Ringer's injection USP, ICU Medical) solutions were administered

throughout the procedure at an average flow rate of 10 mL/Kg/hour. Pupils were dilated with tropicamide 1% (Tropicamide Ophthalmic solution 1% USP, Akron or Sandoz) and phenylephrine 10% (Phenylephrine hydrochloride ophthalmic drops 10%USP, Paragon Biotech). During image acquisition and CR injury, rocuronium (2-3 mg/kg, IV, rocuronium bromide injection 10 mg/mL USP, XGen) was administered and repeated as needed for relaxation of the extraocular muscles. After CR injury, subconjunctival cefazolin (330 mg/mL) 0.4 mL was administered. Upon completion of procedures, an ophthalmic ointment (neomycin and polymyxin B sulfates ophthalmic ointment USP, Bausch and Lomb) was applied on the corneal surface. Ketoprofen (3 mg/kg, IM, Ketofen 100 mg/mL, Zoetis) was administered to reduce pain related to the procedures performed. Fluorescein and indocyanine green were administered intravenously. In preparation for enucleation, pigs were anesthetized using the protocol outlined above. Animals were euthanized by administering B-euthanasia IV 1 mL per 10 lbs of body weight (Euthanasia solution, VetOne) and eyes enucleated. The animal's heart rate, blood pressure, and respiration were monitored to confirm euthanasia.

**Computed Tomography (CT scan) and 3D Skull Reconstruction**

CT scans of the pig head were performed in the Section on Cognitive Neurophysiology and Imaging Laboratory of Neuropsychology (National Institute of Mental Health). An Epica Vimago™ HU Veterinary CT Scanner was used (ARO systems, Australia) to image anesthetized male Yucatan mini pigs. Anatomical Worldwide (Evanston, IL, USA; https://www.anatomicalworldwide.com/) company was contracted to use DICOM set images from the CT scan to design and 3D print the porcine skull. Ballistic gel was purchased from EnvironMolds ART MOLDS (Summit, NJ, USA). It consisted of a 10% non-gelatin clear synthetic gel, which is clear as glass, odorless, reusable, temperature stable (up to 240 F), and mimics human tissue elasticity. The ballistic gel covered the skull and was introduced into the orbit of the

3D printed porcine model to mimic as much as possible the consistency and resistance of the orbital tissue at the time of projectile impact.

**Pressure Application Device (PAD)**

To deliver a small spherical plastic polyoxymethylene (POM) projectile (ball) ø12mm/0.75gr (VXB, Anaheim CA), the PAD consisted of a simple closed pneumatic system, using a compressed gas cylinder to generate precisely measured pressure, triggered by a solenoid-actuated valve (SMC VQ31A1-5YH-C12 4/5 port solénoïde valve, from Automatic Distribution. Hartfield, PA) with a bead loading port and an aiming laser beam for precise delivery to the specific area (Supplementary Fig. 1A and Fig. 1A). The device was connected to a nitrogen tank and a pressure manometer allowing precise control of the exerted pressure (measured in pounds per square inch; PSI). A remote control triggered the projectile (Fig. 1A).

The exit speed of the projectile was measured using a laser photogate and the time-transit method. Collimated laser light (Adafruit 1054, New York, NY) crosses the path of the launch tube's diameter where it illuminates a photodiode (FDS100, Thorlabs, Newton, NJ) masked with a 1.0 mm wide aperture. A transimpedance amplifier (MCP6022, Microchip, Chandler, AZ) converts the photocurrent to a voltage for readout (Supplementary Fig. 1A). A microcontroller and oscilloscope were used to measure the transit-time (t) that the projectile blocked the laser during transit. The diameter (d) of the projectile divided by time (t) yielded the projectile's exit speed ($v=d/t$ in m/s).

**Commotio Retinae (CR) Injury**

Closed-globe CR injury was created under general anesthesia, as described above. The nasal sclera was exposed using 2 limbal traction sutures (6-0 Silk, black braided, Mani, Japan). A

perilimbal nasal peritomy with 2 radial incisions were made in the conjunctiva to expose the medial rectus. Using a muscle hook, the muscle was isolated, its insertion highlighted with tissue marker (Viscot medical, LLC Hanover, NJ) and a double armed suture (6-0 PGA, violet braided, Mani, Japan) passed through the muscle close to the insertion before its disinsertion. Using binocular indirect ophthalmoscopy, the center of the visual streak was identified, and the area of intended impact overlying the visual streak was highlighted using a tissue marker. In latter experiments, to allow for a more posterior impact (to minimize anterior segment damage) and to obtain a more localized and reproducible damage, scleral traction sutures and a commercially available cadaveric human scleral patch thickness ranging from 150-250 micron (Tutoplast processed sclera, Katena Randolph, NJ) glued to the nasal sclera (Fig. 5, Supplementary Fig. 6 ) were used (Vetbond tissue adhesive, 3M St. Paul, MN). After retracting conjunctiva, limbal traction sutures are used to expose nasal sclera. The median rectus is identified; sutured, sectioned and retracted. Scleral sutures are used to further expose nasal sclera. Cadaveric human scleral patch is temporally glued to sclera below median rectus insertion and impact area is highlighted. Once exposed, the PAD laser was aligned with the highlight, with the exit tube 2 inches from the sclera and POM balls at different velocities were tested. After impact, cadaveric sclera is removed, median rectus sutured in its insertion and conjunctiva re-sutured in limbus.

**Optical Coherence Tomography (OCT)**

OCT images were obtained using the Spectralis Spectral-Domain (SD)-OCT (HRA3, Heidelberg Engineering, Germany) instrument and recorded as previously described (52). During each imaging session, three OCT volumes were recorded for each eye: one radial scan (centered in the visual streak) and two raster scans. Raster scans were recorded parallel and perpendicular to the visual streak. To improve signal-to-noise ratio, speckle noise, and contrast, each scan was averaged over 19±2 images with the Automatic Real-time Tracking (ART) function. Radial and

raster scan volumes consisted of up to 48 images and 217 images, respectively. To quantify the effect of the CR injury and the progression of damage, cross-sectional areas of retinal layers were recorded in equally sized OCT-B scans and compared over time on co-registered follow up images. All OCT B-scans were exported in TIFF format using the Heidelberg Eye Explorer 2 (HEYEX 2) software.

**OCT Segmentation**

For segmentation analysis, five cross-sectional areas, evenly divided throughout the OCT volume were analyzed based on our recently developed algorithm (34). The outer border of the visual streak was defined as the borders of the retinal arteries and veins that surround the visual streak. The three equal inner longitudinal lines were used for the analysis (Supplementary Fig 4). To ensure segmented areas were similar at all the time points, the eye tracking device was used in parallel raster scans. All OCT B-scans were manually segmented by an unbiased observer with no prior involvement in the study and the scan export process. Specifically, the inner and outer boundaries of the outer nuclear layer (ONL) were segmented. Annotations were constrained within the visual streak of the pig and outside of scarred regions.

**Segmentation data analysis**

All segmentation files were saved in JSON format. Subsequently, our recently developed MATLAB scripts were used to calculate the axial thickness (34). Axial layer thickness was averaged for each B-scan and was normalized to the corresponding B-scan at baseline. A nonparametric repeated measures ANOVA (Friedman Test) was performed using GraphPad Prism version 9.5.0 for Windows (GraphPad Software, San Diego, California, USA).

## Optical Coherence Tomography Angiography (OCT-A)

Optical coherence tomography angiography (OCT-A) images were obtained using the Spectralis Spectral-Domain (SD) OCT (Heidelberg Engineering, Germany) instrument. Each OCTA B-scan contains between 384 and 768 A-scans and each OCT-A volume contains between 256 and 512 B-scans. OCTA volumes were centered on specific regions of interest (ROIs).

**OCT-A Analysis:** *En face* OCT-A scans were exported from the HEYEX Heidelberg software in TIFF format. Choriocapillaris (CC) vasculature in each CR region was directly compared to CC vasculature in baseline analysis of the same area. An experienced observer obtained the gray value from each *en face* scan, of the average binary pixel intensity, for as big of an area as possible in both CR and baseline regions. All gray value calculations were completed using ImageJ (NIH, Bethesda, MD). For each image, the gray value ratio CR was compared with baseline and was reported as a percent change.

## Fluorescein and Indocyanine Green Angiography (FA, ICGA)

FA and ICGA were obtained using the SD OCT system after intravenous injection of 1 mL Fluorescein 10% solution (AK Fluor 10% USP, Akorn) and 5 mg Indocyanine Green (Indocyanine Green 25 mg USP, Diagnostic Green). A first-minute movie and 1-, 5-, and 10-minutes frames were obtained after the injection.

## Multifocal Electroretinography (mfERG)

The Reti-map-animal mfERG system (Roland Consult, Germany) was used with a 2-channel bio signal amplifier (stimulus frequency selection 10-100Hz) to collect an array of 241 black-and-white hexagons at 10 microvolts over 30 to 40 degrees of the central visual field thus allowing accurate evaluation of the pig visual streak (Supplementary Figure 5). An active contact lens electrode was placed on the cornea using a coupling gel (Genteal® Alcon pharmaceutical, USA). The electrode was connected to an amplifier, and a second electrode was connected to the “ground input" of the amplifier. The pupils were maximally dilated and centered within the ring of the corneal electrode. Recordings were performed under photopic conditions, thus excluding rod contributions to the signal, and ensuring a primarily cone-driven response (52). Considering the variability of the photopic response even within the same day, the Reti-map was set to average three scans for each selected area of the retina.

## Eye Fixation and Sectioning

Cadaveric eyes were fixed in 4% paraformaldehyde for x min immediately after injury and transferred to 1% PBS until histologic processing. Some eyes were open immediately after injury for gross examination before fixation. After fixation, eyes were opened to identify area of interest and send them for histology processing.

Animals were euthanized, and the eyes were collected and processed for histological evaluations. Eyes were fixed for 8 days in paraformaldehyde 2% and glutaraldehyde 2% to maintain tissue morphology, then, placed in 70% Alcohol overnight and washed in running tap water for 24 hours.

During histological processing, retinal retraction on intact sclera was minimized with 15% Alcohol. Absolute ethyl alcohol and water (1:15) mixture was used to pretreat the sections 15 minutes

before transferred to tissue flotation bath and onto glass slides. The solution was freshly prepared (53).

Paraffin-embedded tissues were sectioned at 4-µm-thickness using a Leica microtome (Leica Biosystems- Nussloch, Germany).

Cross sections contained all retinal layers from the *ora serrata* to the posterior pole. Sections were deparaffinized and stained with Harris Hematoxylin and Eosin (H&E), Y Phloxine B to counterstain H&E, and Mason trichromic (Stat lab-USA).

**Immunostaining of paraffin sections**

Deparaffinization was performed as previously described(54) followed by Antigen retrieval (water bath 2x/Citrate Buffer 1X pH 6.0) pre heated in steamer (Life Technology #005000, Thermo Fisher Scientific-US) for 15 minutes followed by: Primary antibody incubation was performed overnight at room temperature. The following primary antibodies were used RPE65 mouse Ab 1:500 (Abcam Cat# ab175936, Abcam Inc., UK), peanut agglutinin (PNA) 5mg 1:500 (FL-1075-5) conjugated with a 488 fluorophore. Secondary antibody Alexa fluor 568 1:300 (Invitrogen, Thermo Fisher Scientific, USA) was incubated for 30 min at room temperature. Sections were also stained with Hoechst 33342 1:1000 (Cat# 62249 Invitrogen, Thermo Fisher Scientific-USA).

**Statistical Analysis**

For average velocities analysis, GraphPad Prism version 9.5.0 was also used, and results were analyzed using one-way ANOVA.

## Study Approval

All animal procedures were performed in accordance with the guidelines of the Association for Research in Vision and Ophthalmology statement for the use of animals in ophthalmic and vision research. All animal procedures received prior approval from the National Eye Institute, NIH, Animal Care and Use Committee.

## Author contributions

JA, IB, AM, MMC, FB, RG, MF, JN developed and tested the CR porcine model. MJP, RS, DMG, KB, ABD RJB contributed to study design, data analysis, and manuscript writing. KB approved the manuscript.

The authors have declared that no conflict of interest exists.

## Data availability

Raw values are provided in Supporting Data Values file in supplementary material. Segmented JSON files for OCT are available from the corresponding author upon request.

## Disclosure

The authors report no proprietary or commercial interest in any product mentioned or concept discussed in this article.

This work is the result of Intramural Research Program NIH funding, in whole or in part, and is subject to the NIH Public Access Policy. Through acceptance of this federal funding, the NIH has been given a right to make the work publicly available in PubMed Central.

The contributions of the NIH authors were made as part of their official duties as NIH federal employees, follow agency policy requirements, and are considered Works of the United States

Government. However, the findings and conclusions presented in this paper are those of the author(s) and do not necessarily reflect the views of the NIH or the U.S. Department of Health and Human Services.

**Acknowledgments**

This work was supported by NEI IRP funds to KB and by a Department of Defense (DoD) grant W81XWH-20-1-0655 to DMG and KB, and Research to Prevent Blindness (DMG). Dr. Haohua Qian head of the visual function core at the NEI for his invaluable help with the OCT set up and evaluations and Dr. Krystal Allen-Worthington, head of the NEI Veterinary Research and Resources Section for her help for performing the pig MRI.

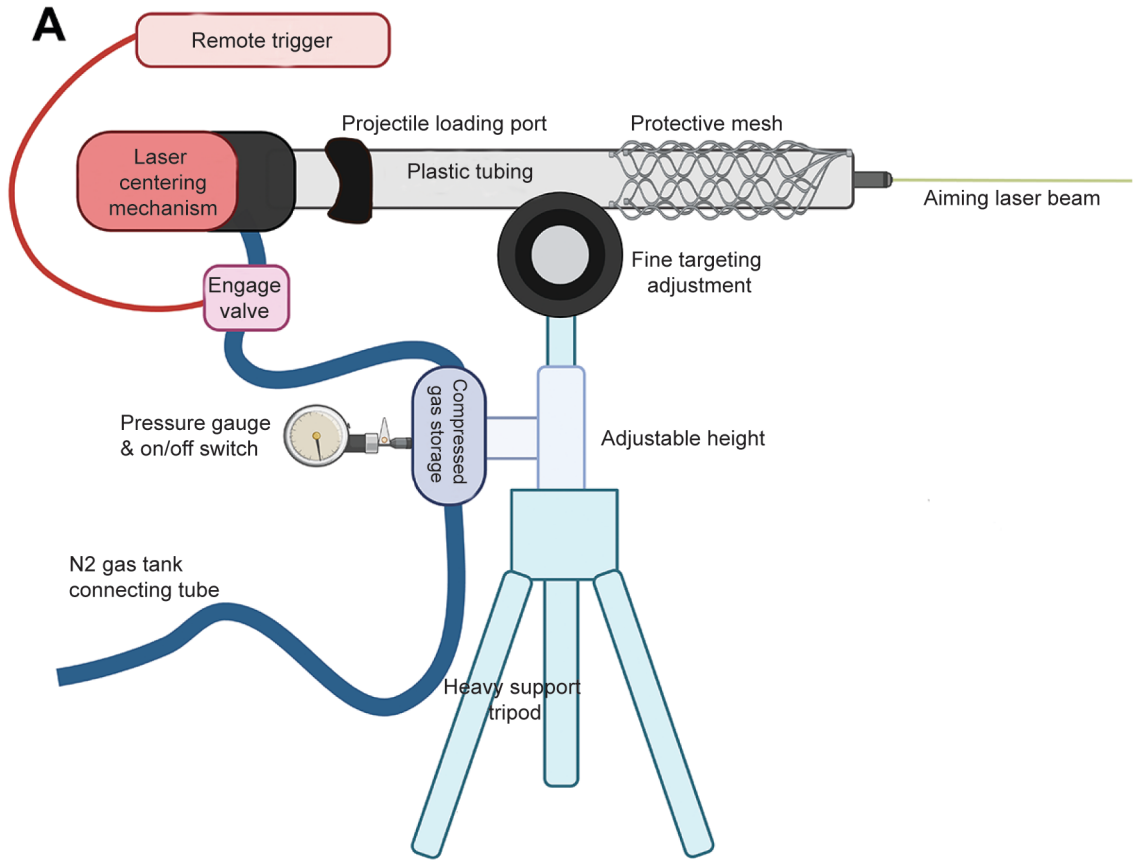
A
Remote trigger
Laser centering mechanism
Projectile loading port
Protective mesh
Plastic tubing
Aiming laser beam
Fine targeting adjustment
Engage valve
Compressed gas storage
Pressure gauge & on/off switch
Adjustable height
N2 gas tank connecting tube
Heavy support tripod

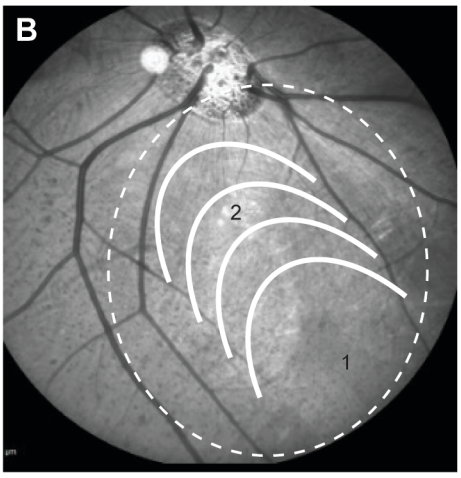
B
2
1

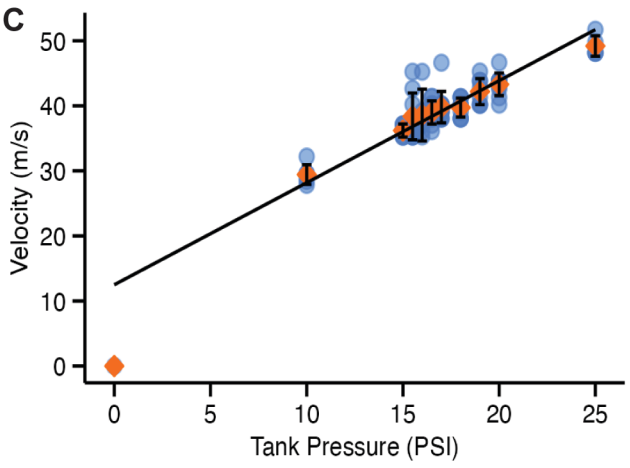
C
Velocity (m/s)
0
10
20
30
40
50
0
5
10
15
20
25
Tank Pressure (PSI)

**Figure 1. Development of a pressure application device (PAD) for inducing closed globe commotio retinae (CR) in porcine eyes. (A)** The PAD contains a plastic tube, a projectile loading port, and an aiming laser beam. PAD connects to a nitrogen tank, and a pressure manometer, allowing control of pressure (measured in PSI) used to propel the projectile (ø12mm/0.75g). A remote trigger releases the pressure to propel the projectile. **(B)** Porcine fundus infrared photograph showing the visual streak (white dotted circle); (1) the site of projectile impact on peripheral retina; (2) semicircles show the projected path of the shockwave generated by the impact, leading to an indirect visual streak damage. **(C)** Graph shows the average of projectile speed (m/s) measurements as a function of nitrogen gas pressures (psi) ranging from 10.0 to 25.0 psi (gauge pressure). Results were analyzed using one-way ANOVA. The standard deviation of the mean was used to estimate uncertainty in projectile speed for each tank pressure.

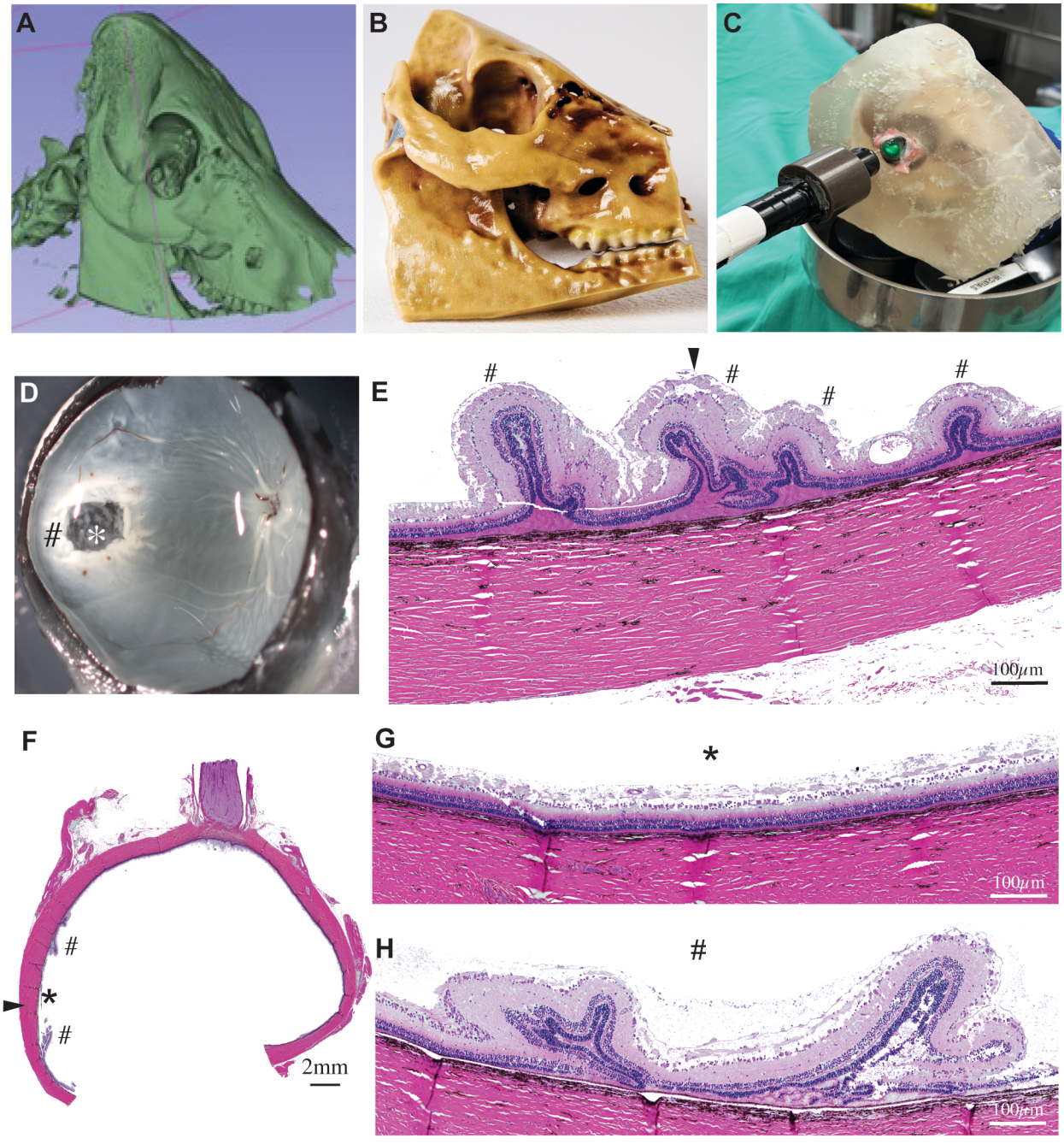
A
B
C
D
#
*
E
#
#
#
#
100μm
F
#
*
#
2mm
G
*
100μm
H
#
100μm

**Figure 2. *Ex vivo* evaluation of commotio retinae (CR) injury using 3D-printed porcine skull.** **(A)** Computed tomography scan assisted 3D rendering of a pig skull. **(B)** 3D-printed model of a pig skull from 3D rendering generated in (A). **(C)** 3D-printed pig skull with a fitted cadaveric pig eye in the orbit along with non-gelatin based 10% ballistic gel®. Pressure application device (PAD) aimed at the cadaveric pig eye (arrowhead). **(D)** Gross specimen view after the CR injury showing the impact area in the sclera (*) and a surrounding whitened area (#). **(E)** Hematoxylin & Eosin (H&E) stained sections from retinal region corresponding to the corneal impact (#) showing retinal folds in the visual streak. Arrowhead shows the impact direction in the cornea. **(F)** H&E-stained eye section showing the scleral impact zone (black arrowhead), impacted retina (*) in lower (F) and higher **(G)** magnifications, and retinal region with folds (#) surrounding the impact area, in lower (F) and higher **(H)** magnifications. N = 3 eyes per condition.

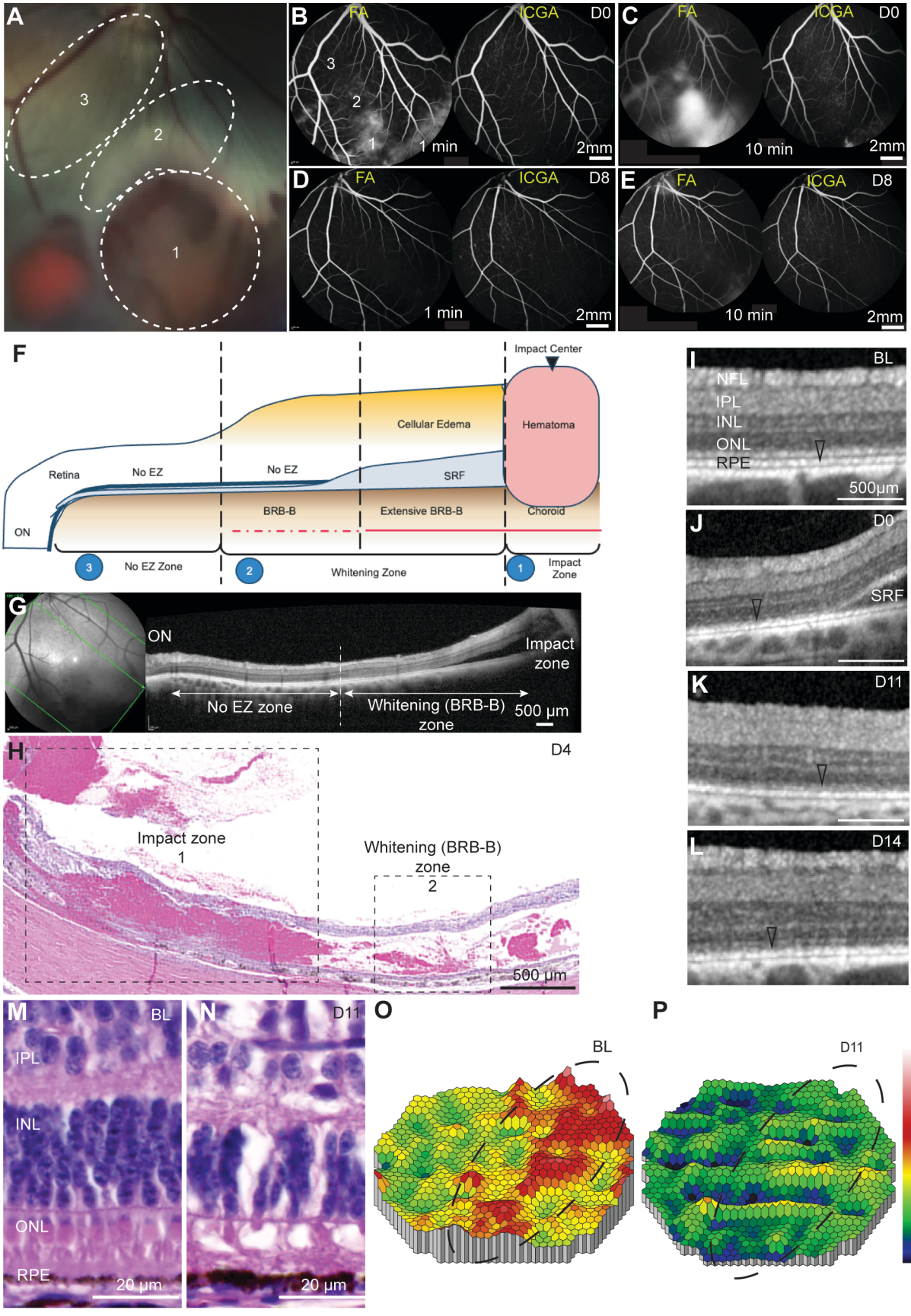
A
3
2
1
B
FA
ICGA
D0
1 min
2mm
C
FA
ICGA
D0
10 min
2mm
D
FA
ICGA
D8
1 min
2mm
E
FA
ICGA
D8
10 min
2mm
F
Impact Center
Cellular Edema
Hematoma
Retina
No EZ
No EZ
SRF
BRB-B
Extensive BRB-B
Choroid
ON
No EZ Zone
Whitening Zone
Impact Zone
G
ON
Impact zone
No EZ zone
Whitening (BRB-B) zone
500 µm
H
D4
Impact zone 1
Whitening (BRB-B) zone 2
500 µm
I
BL
NFL
IPL
INL
ONL
RPE
500µm
J
D0
SRF
K
D11
L
D14
M
BL
IPL
INL
ONL
RPE
20 µm
N
D11
20 µm
O
BL
P
D11
0.35
µV
0.0

**Figure 3. Short term evaluation of pig eyes with CR injury. (A)** High magnification of color fundus photograph of CR injured eye showing: preretinal hemorrhage at the impact site (1), the whitening zone (2), and the adjacent visual streak (3). **(B-E)** Fluorescein angiography (FA) (left panels) images showing fluorescein dye leakage in early phase (1 min) on day 0 **(B)** and late phase (10 min) on day 0 post injury **(C)**, but not on day 8 post injury (**D** – early phase or **E** - late phase); (**B, C, D, E**) Indocyanine, green angiography (ICGA) images (right panels) show no dye leakage on day 0 post injury (**B** – early phase or **C** – late phase) and day 8 (**D** – early phase or **E**– late phase). **(F)** Schematic depicting the three distinct zones seen on color fundus and OCT images – impact zone showing hematoma (zone 1); whitening zone with extensive oBRB damage and subretinal fluid (SRF) accumulation (zone 2), and zone with ellipsoid zone (EZ) disruption (zone 3). **(G, H)** OCT **(G)** and (H&E staining **(H)** depicting the three zones described in **F**. **(I-L)** Higher magnification OCT images at baseline (bl) showing the ellipsoid zone **(arrow head, I)**; subretinal fluid (SRF) accumulation on day 0 after the CR injury **(J)**; fluid resorption by day 11 but missing ellipsoid zone (arrowhead) **(K),** which persists on day 14 **(L)**. **(M, N)** Hematoxylin & Eosin (H&E) section depicting healthy retina at baseline (Bl) **(M)**, and disruptions ONL and photoreceptor outer segments (arrowhead) 11 days after CR injury **(N)**. **(O, P)** mfERG signal heatmap at baseline (bl) (**O)** and day 11 (D11) **(P)** post-injury showing the visual streak (vs) and surrounding areas retina light response. Nine eyes were used for short term evaluation of CR injury. NFL- Nerve Fiber Layer, IPL- Inner Plexiform Layer, INL- Inner Nuclear Layer, ONL- Outer Nuclear Layer, RPE- Retinal Pigment Epithelium.

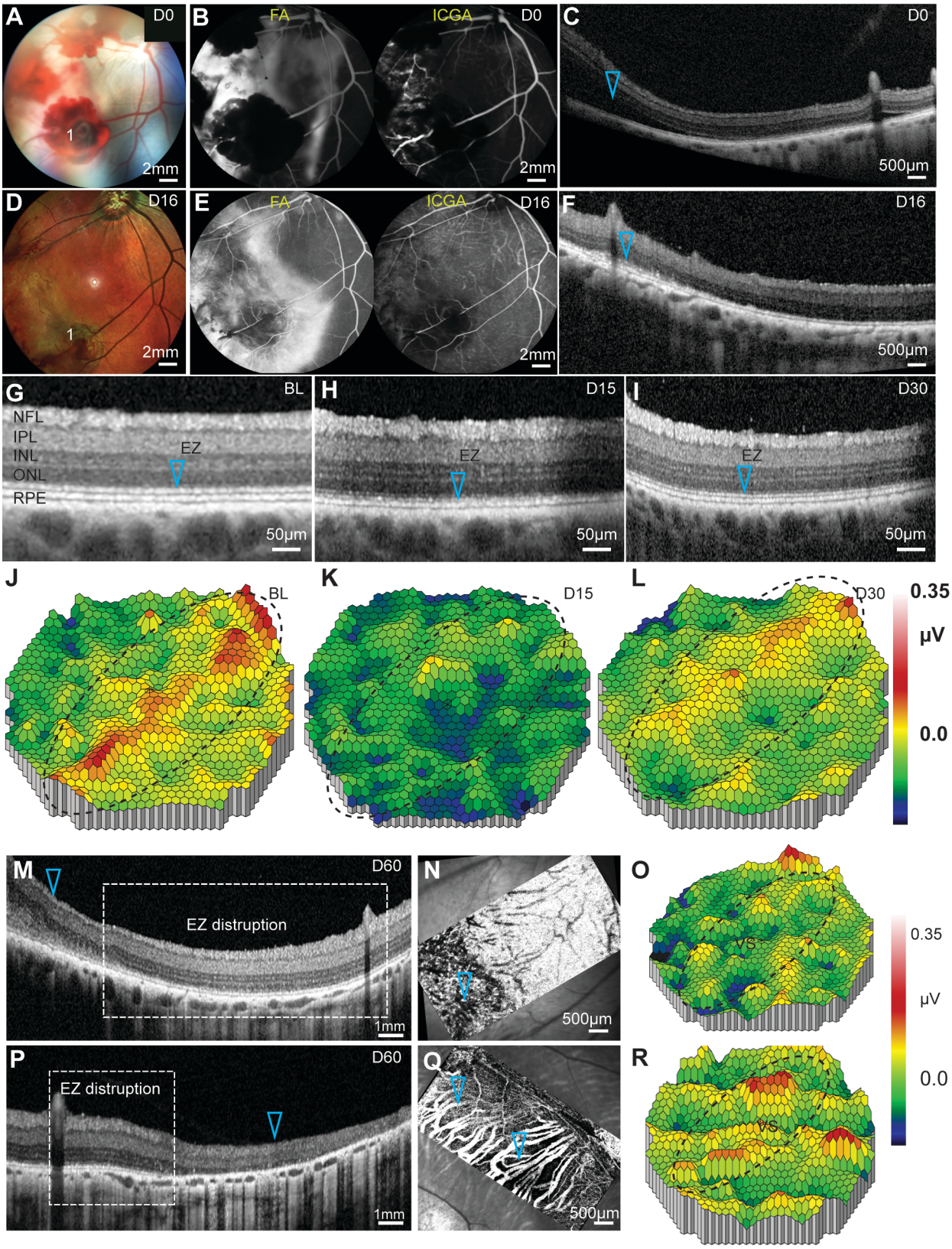
A
D0
1
2mm
B
FA
ICGA
D0
2mm
C
D0
500μm
D
D16
1
2mm
E
FA
ICGA
D16
2mm
F
D16
500μm
G
BL
NFL
IPL
INL
ONL
RPE
EZ
50μm
H
D15
EZ
50μm
I
D30
EZ
50μm
J
BL
K
D15
L
D30
0.35
μV
0.0
M
D60
EZ distruption
1mm
N
500μm
O
VS
0.35
μV
0.0
P
D60
EZ distruption
1mm
Q
500μm
R
VS

**Figure 4. CR injury recovery in the long-term evaluation.** Color fundus **(A, D)**, late phase (10 min) fluorescein angiography - FA **(B, E – left panels)**, indocyanine green angiography (ICGA) **(B, E – right panels)**, and OCT **(C, F)** of post-injury eyes on day 0 **(A-C)** and day 16 **(D-F)** of evaluation of the same eye. One (1) marks the area of impact showing preretinal hemorrhage. Whitened area in color fundus images corresponds to sub retinal fluid accumulation on day 0, which is resolved by day 16 (arrowhead in **C, F**). **(G-L)** OCT **(G-I)** and mfERG **(J-L)** analysis shows recovery of ellipsoid zone (compare arrowheads in G-I) and recovery of mfERG signal in the visual streak (dotted oval) **(J-L)** by day 30 in eyes injured with a projective speed of 35.7 m/s. **(M-R)** Comparative analysis at 60 days post injury using OCT **(M, P)**, OCT-angiography **(N, Q)**, and mfERG **(O, R)** of two eyes injured with a projectile speed of 39.5m/s highlights variability in damage to the outer retina to the ellipsoid zone (EZ) (arrowheads in **M and N**), to the choriocapillaris (arrowheads in **N and Q**), and the variable signal in the visual streak (VS – dotted circle) **(O, R)**. Seven eyes were used for this evaluation.

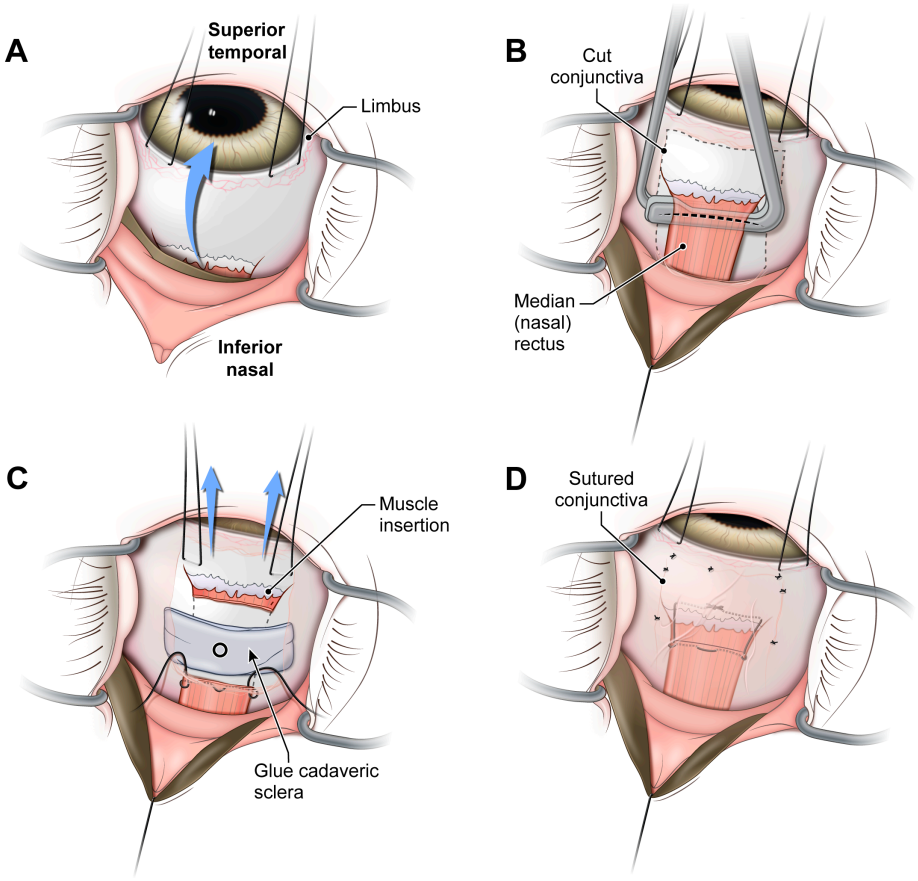
A
Superior temporal
Limbus
Inferior nasal
B
Cut conjunctiva
Median (nasal) rectus
C
Muscle insertion
Glue cadaveric sclera
D
Sutured conjunctiva

**Figure 5. Surgical technique for cadaveric scleral patch placement. (A)** Nasal sclera is exposed using limbal traction sutures. **(B)** Nasal conjunctiva is cut to expose and isolate the median rectus muscle using hooks. Mark the area where muscle would be cut (dotted line). **(C)** Scleral traction sutures are used to increase exposure of nasal sclera. A piece of cadaveric sclera is temporally glued to the sclera, and the area of impact is marked (black circle). **(D)** After impact, the cadaveric sclera is removed, median rectus muscle is sutured back to its insertion and conjunctiva is replaced and sutured (also see supplementary Fig. 6).

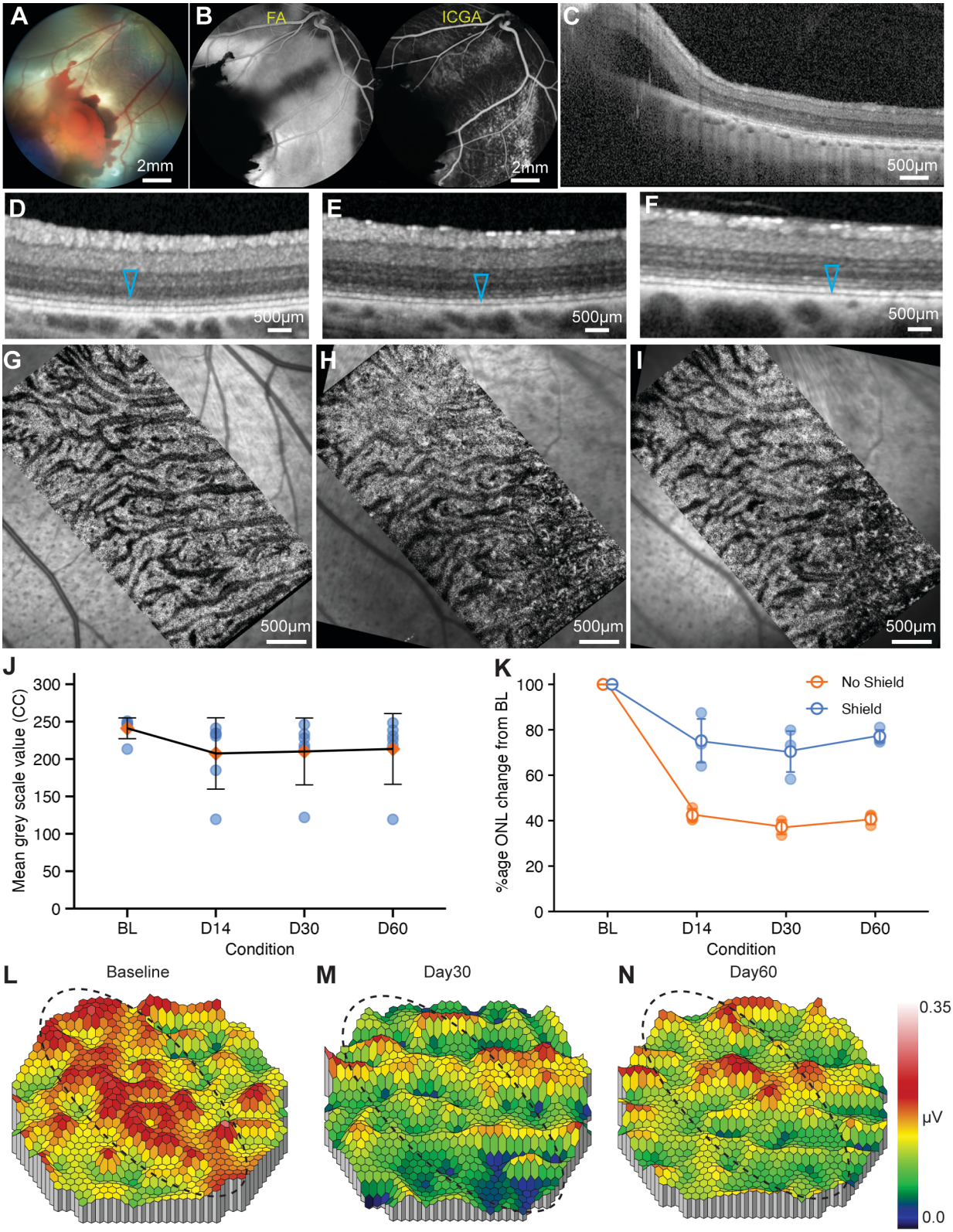
A
2mm
B
FA
ICGA
2mm
C
500µm
D
500µm
E
500µm
F
500µm
G
500µm
H
500µm
I
500µm
J
Mean grey scale value (CC)
300
250
200
150
100
50
0
BL
D14
D30
D60
Condition
K
%age ONL change from BL
100
80
60
40
20
0
No Shield
Shield
BL
D14
D30
D60
Condition
L
Baseline
M
Day30
N
Day60
0.35
µV
0.0

**Figure 6. Long term evaluation of CR injury caused using a cadaveric scleral patch. (A-C)** Color fundus image **(A)** showing the area of impact with preretinal hemorrhage and the surrounding area of retinal whitening. **(B)** Late phase (10 min) FA and ICGA show blocked fluorescence signal due to hemorrhage. **(C)** OCT showing subretinal fluid (SRF) corresponding to the whitening area in (A). **(D-I)** OCT images **(D-F)** and corresponding OCT-A images **(G-I)** depicting the presence of ellipsoid zone and choriocapillaris respectively at baseline (**D**, arrowhead) and clear ellipsoid zone absence at 30 days (**E**, arrowhead) and 60 days (**F**, arrowhead) post-injury. Minimal changes are seen in choriocapillaris (compare G-I, arrowheads). **(J)** Median grayscale values intensity graph of OCT-A signal intensity up to 60 days after CR injury. Results were analyzed using one-way ANOVA. **(K)** Graph showing ONL thickness at baseline, 15, 30, and 60 days after projectile impact at 39.5 m/s on eyes with no scleral patch vs with scleral pact impacts. Data is presented as a percentage of average thickness of the same location at baseline. ANOVA (Friedman Test compared to baseline) was used for statistical analysis. * $p<0.05$, ** $p<0.01$. **(L-N)** mfERG heatmaps at baseline **(L)**, 30 days **(M)**, and 60 days **(N)** after CR injury depicting changes in mfERG sensitivity throughout the evaluation time. Visual streak is highlighted by dotted oval circles. Four eyes were used for this evaluation.

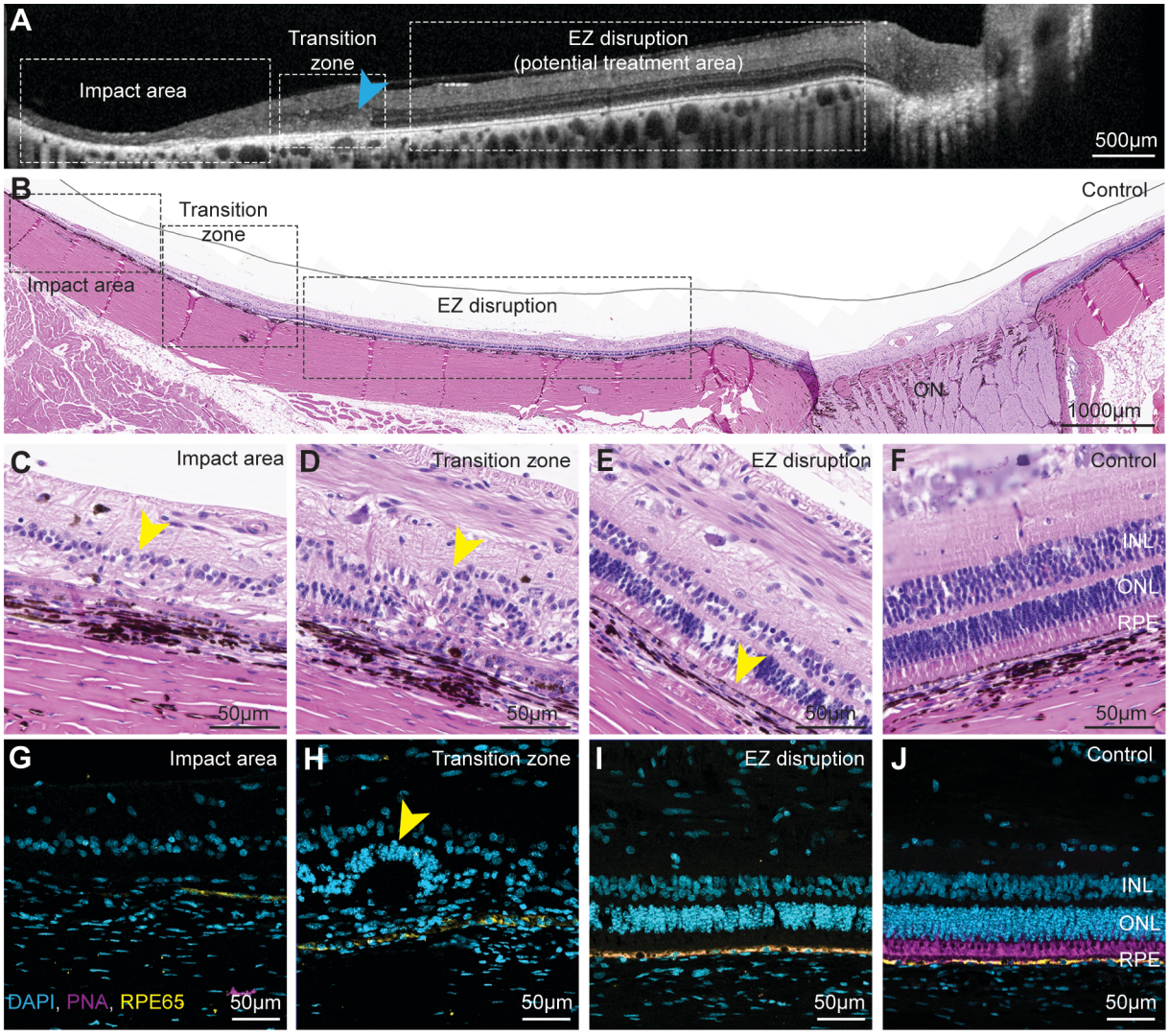
A
Transition zone
EZ disruption (potential treatment area)
Impact area
500μm
B
Control
Transition zone
Impact area
EZ disruption
ONL
1000μm
C
Impact area
50μm
D
Transition zone
50μm
E
EZ disruption
50μm
F
Control
INL
ONL
RPE
50μm
G
Impact area
DAPI, PNA, RPE65
50μm
H
Transition zone
50μm
I
EZ disruption
50μm
J
Control
INL
ONL
RPE
50μm

**Figure 7. Histological analysis of CR model porcine eyes. (A, B)** Terminal point OCT **(A, arrow marks the transition zone)** and corresponding H&E-stained section **(B)** showing the impact area with complete retinal atrophy, the transition zone with significant outer retina damage, and an area with ellipsoid zone disruption. **(C-K)** Higher magnification views of the impact area **(C, G)** showing complete retinal atrophy (arrow head), the transition zone **(D, H)** showing outer and inner retina layer degeneration (arrow heads), **(E, I)** showing degenerated photoreceptor outer segments and missing EX band (arrow heads) with relatively preserved photoreceptor outer nuclear layer, and control retina **(F, K)** stained with H&E (panels **C-F**) or stained for cone photoreceptors (PNA – magenta), RPE (RPE65-yellow) and nuclei (DAPI-cyan) (panels **G-K**).

## References


1. Swain T, and McGwin G, Jr. The Prevalence of Eye Injury in the United States, Estimates from a Meta-Analysis. *Ophthalmic Epidemiol.* 2020;27(3):186-93.
2. Kuhn F, Morris R, Witherspoon CD, and Mann L. Epidemiology of blinding trauma in the United States Eye Injury Registry. *Ophthalmic Epidemiol.* 2006;13(3):209-16.
3. Mir TA, Canner JK, Zafar S, Srikumaran D, Friedman DS, and Woreta FA. Characteristics of open globe injuries in the United States from 2006 to 2014. *JAMA ophthalmology.* 2020;138(3):268-75.
4. Bourne RR, Stevens GA, White RA, Smith JL, Flaxman SR, Price H, et al. Causes of vision loss worldwide, 1990–2010: a systematic analysis. *The lancet global health.* 2013;1(6):e339-e49.
5. Négrel A-D, and Thylefors B. The global impact of eye injuries. *Ophthalmic epidemiology.* 1998;5(3):143-69.
6. Alexander DA, Kemp RV, Klein S, and Forrester JV. Psychiatric sequelae and psychosocial adjustment following ocular trauma: a retrospective pilot study. *Br J Ophthalmol.* 2001;85(5):560-2.
7. Flatter JA, Cooper RF, Dubow MJ, Pinhas A, Singh RS, Kapur R, et al. Outer retinal structure after closed-globe blunt ocular trauma. *Retina.* 2014;34(10):2133-46.
8. Blanch RJ, Good PA, Shah P, Bishop JR, Logan A, and Scott RA. Visual outcomes after blunt ocular trauma. *Ophthalmology.* 2013;120(8):1588-91.
9. Eagling EM. Ocular damage after blunt trauma to the eye. Its relationship to the nature of the injury. *The British journal of ophthalmology.* 1974;58(2):126.
10. Weichel ED, Colyer MH, Ludlow SE, Bower KS, and Eiseman AS. Combat ocular trauma visual outcomes during operations iraqi and enduring freedom. *Ophthalmology.* 2008;115(12):2235-45.
11. Spraul CW, and Grossniklaus HE. Vitreous hemorrhage. *Survey of ophthalmology.* 1997;42(1):3-39.
12. Jones N, Hayward J, Khaw P, Claoué C, and Elkington A. Function of an ophthalmic" accident and emergency" department: results of a six month survey. *Br Med J (Clin Res Ed).* 1986;292(6514):188-90.
13. Blanch RJ, Ahmed Z, Thompson AR, Akpan N, Snead DR, Berry M, et al. Caspase-9 mediates photoreceptor death after blunt ocular trauma. *Invest Ophthalmol Vis Sci.* 2014;55(10):6350-7.
14. Wolter JR. Coup-contrecoup mechanism of ocular injuries. *American journal of ophthalmology.* 1963;56(5):785-96.
15. Blanch RJ, Ahmed Z, Sik A, Snead DR, Good PA, O'Neill J, et al. Neuroretinal cell death in a murine model of closed globe injury: pathological and functional characterization. *Invest Ophthalmol Vis Sci.* 2012;53(11):7220-6.
16. Blanch RJ, Ahmed Z, Berry M, Scott RA, and Logan A. Animal models of retinal injury. *Invest Ophthalmol Vis Sci.* 2012;53(6):2913-20.
17. Blight R, and Hart J. Structural changes in the outer retinal layers following blunt mechanical non-perforating trauma to the globe: an experimental study. *British Journal of Ophthalmology.* 1977;61(9):573-87.
18. Bunt-Milam AH, Black RA, and Bensinger RE. Breakdown of the outer blood-retinal barrier in experimental commotio retinae. *Experimental eye research.* 1986;43(3):397-412.
19. Cox MS. Retinal breaks caused by blunt nonperforating trauma at the point of impact. *Transactions of the American Ophthalmological Society.* 1980;78:414.
20. Gregor Z, and Ryan SJ. Blood-retinal barrier after blunt trauma to the eye. *Graefe's Archive for Clinical and Experimental Ophthalmology.* 1982;219:205-8.

21. Gregor Z, and Ryan SJ. Combined posterior contusion and penetrating injury in the pig eye. I. A natural history study. *The British Journal of Ophthalmology.* 1982;66(12):793.
22. Hart JC, and Blight R. Early changes in peripheral retina following concussive ocular injuries: an experimental study. *J R Soc Med.* 1979;72(3):180-4.
23. Hui YN, Wu YQ, Xiao QS, Kirchhof B, and Heimann K. Repair of outer blood-retinal barrier after severe ocular blunt trauma in rabbits. *Graefes Arch Clin Exp Ophthalmol.* 1993;231(6):365-9.
24. Kohno T, Ishibashi T, Inomata H, Ikui H, and Taniguchi Y. Experimental macular edema of commotio retinae: preliminary report. *Jpn J Ophthalmol.* 1983;27(1):149-56.
25. LATANZA L, ALFARO DV, BOCKMAN R, IWAMOTO T, HEINEMANN M-H, and CHANG S. Leukotrienes levels in the aqueous humor following experimental ocular trauma. *Retina.* 1988;8(3):199-204.
26. Liu Y, Yang T, Yu J, Li M, Li J, and Yan H. Creation of a new explosive injury equipment to induce a rabbit animal model of closed globe blast injury via gas shock. *Frontiers in Medicine.* 2021;8:749351.
27. Sipperley JO, Quigley HA, and Gass JDM. Traumatic retinopathy in primates: the explanation of commotio retinae. *Archives of Ophthalmology.* 1978;96(12):2267-73.
28. Berlin R. Zur sogenannten Commotio retinaw. *Klin Mbl Augenheilk.* 1873;11:42-78.
29. PULIDO JS, and BLAIR NP. The blood-retinal barrier in Berlin's edema. *Retina.* 1987;7(4):233-6.
30. Hart J, and Frank H. Retinal opacification after blunt non-perforating concussional injuries to the globe. A clinical and retinal fluorescein angiographic study. *Transactions of the ophthalmological societies of the United Kingdom.* 1975;95(1):94-100.
31. De Schaepdrijver L, Simoens P, Lauwers H, and De Geest JP. Retinal vascular patterns in domestic animals. *Res Vet Sci.* 1989;47(1):34-42.
32. Sanchez I, Martin R, Ussa F, and Fernandez-Bueno I. The parameters of the porcine eyeball. *Graefes Arch Clin Exp Ophthalmol.* 2011;249(4):475-82.
33. Sharma R, Khristov V, Rising A, Jha BS, Dejene R, Hotaling N, et al. Clinical-grade stem cell-derived retinal pigment epithelium patch rescues retinal degeneration in rodents and pigs. *Sci Transl Med.* 2019;11(475).
34. Gupta R, Bunea I, Alvisio B, Barone F, Gupta R, Baker D, et al. iPSC-RPE patch restores photoreceptors and regenerates choriocapillaris in a pig retinal degeneration model. *JCI Insight.* 2025;10(10).
35. Ross JW, Fernandez de Castro JP, Zhao J, Samuel M, Walters E, Rios C, et al. Generation of an inbred miniature pig model of retinitis pigmentosa. *Invest Ophthalmol Vis Sci.* 2012;53(1):501-7.
36. Winkler PA, Occelli LM, and Petersen-Jones SM. Large animal models of inherited retinal degenerations: a review. *Cells.* 2020;9(4):882.
37. Blight R, and Hart J. Histological changes in the internal retinal layers produced by concussive injuries to the globe. An experimental study. *Transactions of the Ophthalmological Societies of the United Kingdom.* 1978;98(2):270-7.
38. Oh J, Jung J-H, Moon SW, Song SJ, Yu HG, and Cho HY. Commotio retinae with spectral-domain optical coherence tomography. *Retina.* 2011;31(10):2044-9.
39. Ahn SJ, Woo SJ, Kim KE, Jo DH, Ahn J, and Park KH. Optical coherence tomography morphologic grading of macular commotio retinae and its association with anatomic and visual outcomes. *American journal of ophthalmology.* 2013;156(5):994-1001. e1.
40. Mendes S, Campos A, Campos J, Neves A, Beselga D, Fernandes C, and Sousa JPC. Cutting edge of traumatic maculopathy with spectral-domain optical coherence tomography–A review. *Medical Hypothesis, Discovery and Innovation in Ophthalmology.* 2015;4(2):56.

41. Chen H, Lu Y, Huang H, Zheng J, Hou P, and Chen W. Prediction of visual prognosis with spectral-domain optical coherence tomography in outer retinal atrophy secondary to closed globe trauma. *Retina.* 2013;33(6):1258-62.
42. Souza-Santos F, Lavinsky D, Moraes NS, Castro AR, Cardillo JA, and Farah ME. Spectral-domain optical coherence tomography in patients with commotio retinae. *Retina.* 2012;32(4):711-8.
43. Noia Lda C, Berezovsky A, Freitas D, Sacai PY, and Salomão SR. [Clinical and electroretinographic profile of commotio retinae]. *Arq Bras Oftalmol.* 2006;69(6):895-906.
44. Olsen TW, Sanderson S, Feng X, and Hubbard WC. Porcine sclera: thickness and surface area. *Invest Ophthalmol Vis Sci.* 2002;43(8):2529-32.
45. Hart JC, and Blight R. Commotio retinae. *Arch Ophthalmol.* 1979;97(9):1738.
46. Kohno T, Miki T, and Hayashi K. Choroidopathy after blunt trauma to the eye: a fluorescein and indocyanine green angiographic study. *American journal of ophthalmology.* 1998;126(2):248-60.
47. Ludwig CA, Shields RA, Do DV, Moshfeghi DM, and Mahajan VB. Traumatic chorioretinitis sclopetaria: Risk factors, management, and prognosis. *American Journal of Ophthalmology Case Reports.* 2019;14:39-46.
48. Itakura H, and Kishi S. Restored photoreceptor outer segment in commotio retinae. *Ophthalmic Surgery, Lasers, and Imaging.* 2011;42(6):e29-e31.
49. Knighton RW, and Blankenship GW. Electrophysiological evaluation of eyes with opaque media. *Int Ophthalmol Clin.* 1980;20(1):1-19.
50. Mansour AM, Green WR, and Hogge C. Histopathology of commotio retinae. *Retina.* 1992;12(1):24-8.
51. Fernandez de Castro JP, Scott PA, Fransen JW, Demas J, DeMarco PJ, Kaplan HJ, and McCall MA. Cone photoreceptors develop normally in the absence of functional rod photoreceptors in a transgenic swine model of retinitis pigmentosa. *Invest Ophthalmol Vis Sci.* 2014;55(4):2460-8.
52. Barone F, Amaral J, Bunea I, Farnoodian M, Gupta R, Gupta R, et al. A versatile laser-induced porcine model of outer retinal and choroidal degeneration for preclinical testing. *JCI Insight.* 2023;8(11).
53. Kumar N, Nayak B, Somayaji S, Nayak S, KUMAR N, NAYAK B, et al. Role of dilute alcohol in the removal of fine wrinkles from paraffin sections, a Histo-technical study. *Int J Morphol.* 2012;30:45-8.
54. Prophet EB. *Laboratory methods in histotechnology.* American registry of pathology; 1992.